

*Erik Jonsson School of Engineering and Computer Science*

***Tuning Electronic Transport in Epitaxial Graphene-  
Based Van Der Waals Heterostructures—Supplement***

©2016 The Royal Society of Chemistry. This article may not be further made available or distributed.

**Citation:**

Lin, Yu-Chuan, Jun Li, Sergio, C. de la Barrera, Sarah M. Eichfeld, et al. 2016. "Tuning electronic transport in epitaxial graphene-based van der Waals heterostructures." *Nanoscale* 8, doi: 10.1039/C6NR01902A

*This document is being made freely available by the Eugene McDermott Library of The University of Texas at Dallas with permission from the copyright owner. All rights are reserved under United States copyright law unless specified otherwise.*

## **Supplementary Information**

# **Tuning Electronic Transport in Epitaxial Graphene-based van der Waals Heterostructures**

Yu-Chuan Lin,<sup>a</sup> Jun Li,<sup>b</sup> Sergio C. de la Barrera,<sup>b</sup> Sarah M. Eichfeld,<sup>a</sup> Yifan Nie,<sup>c</sup> Rafik Addou,<sup>c</sup> Patrick C. Mende,<sup>b</sup> Robert M. Wallace,<sup>c</sup> Kyeongjae Cho,<sup>c</sup> Randall M. Feenstra,<sup>b</sup> and Joshua A. Robinson<sup>a,\*</sup>

<sup>a</sup>Department of Materials Science and Engineering and Center for 2-Dimensional and Layered Materials,  
The Pennsylvania State University, University Park, PA 16802 USA

<sup>b</sup>Department of Physics, Carnegie Mellon University, Pittsburgh, PA 15213 USA

<sup>c</sup>Department of Materials Science and Engineering, The University of Texas at Dallas, Richardson, Texas  
75080, USA

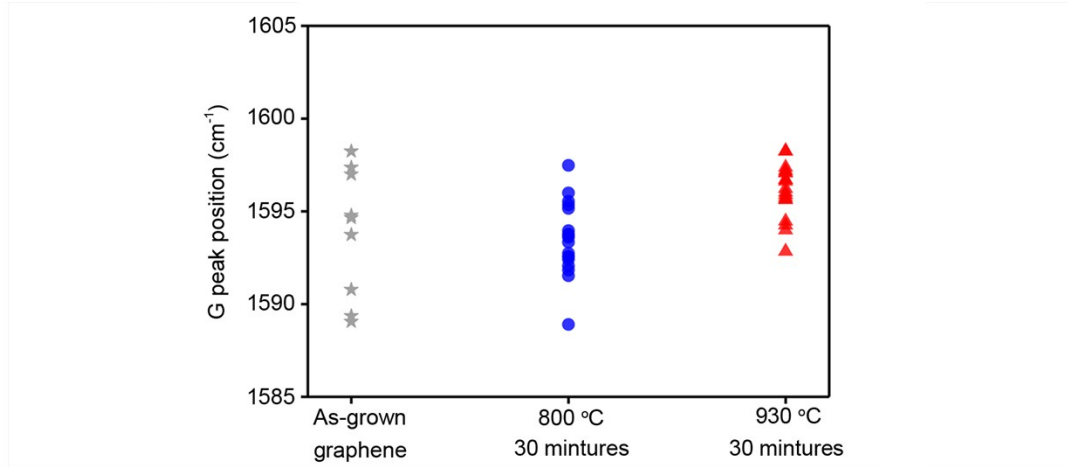
\* E-mail: [jrobinson@psu.edu](mailto:jrobinson@psu.edu)

Methods	PV <sup>1</sup> WSe <sub>2</sub> /EG	MOCVD WSe <sub>2</sub> /EG (Sample 1)	MOCVD WSe <sub>2</sub> /EG (Sample 2)
WSe <sub>2</sub> growth conditions	5 % H <sub>2</sub> /Ar 5 -10 Torr 925 °C 30 mins.	100 % H <sub>2</sub> 700 Torr 800 °C 30 mins.	100 % H <sub>2</sub> 700 Torr 800 °C 30 mins.
C 1s of EG	284.1 eV	284.1 eV	284.1 eV
C 1s of EG after WSe <sub>2</sub> growth	284.4 eV (+ 0.3 eV)	284.0 eV (- 0.1 eV)	284.0 eV (- 0.1 eV)

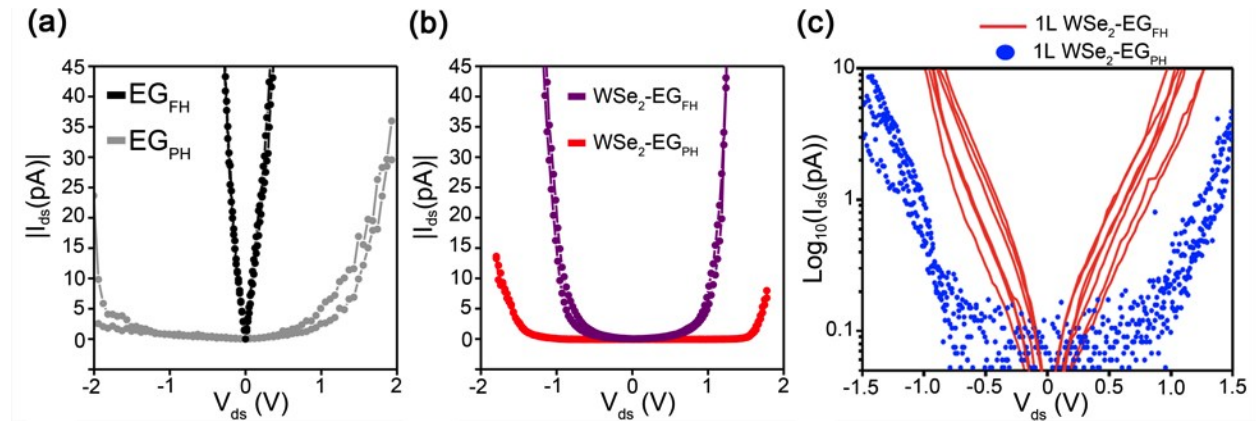
**Supplementary Table 1.** Binding energy of C1s, which is corresponding to the C-C sp<sup>2</sup> from the epitaxial graphene (EG) used as template in powder vaporization (PV) and metal-organic chemical vapor deposition (MOCVD) for WSe<sub>2</sub> synthesis show the MOCVD process, carried out in a pure H<sub>2</sub> atmosphere, significantly shifts the C1s of WSe<sub>2</sub>-EG towards a lower binding energy (This work, highlighted in the table). The C 1s of EG without exposure to WSe<sub>2</sub> synthesis is used as a reference.

$X_{EG_{PH}}$ (eV)	$X_{EG_{FH}}$ (eV)	$X_{WSe_2} + E_g$ (eV)	$N_A$ (cm <sup>-2</sup> )	$N_{C,WSe_2-EG_{PH}}$ (cm <sup>-2</sup> )	$N_{C,WSe_2-EG_{FH}}$ (cm <sup>-2</sup> )
4.57	4.71	5.09	1.3x10 <sup>12</sup>	4.1x10 <sup>5</sup>	2.9x10 <sup>12</sup>
4.47	4.71	5.09	1.3x10 <sup>12</sup>	0.9x10 <sup>4</sup>	2.9x10 <sup>12</sup>
4.67	4.71	5.09	1.3x10 <sup>12</sup>	2.0x10 <sup>7</sup>	2.9x10 <sup>12</sup>
4.57	4.61	4.99	1.3x10 <sup>12</sup>	2.0x10 <sup>7</sup>	2.9x10 <sup>12</sup>
4.57	4.81	5.19	1.3x10 <sup>12</sup>	0.9x10 <sup>4</sup>	2.9x10 <sup>12</sup>

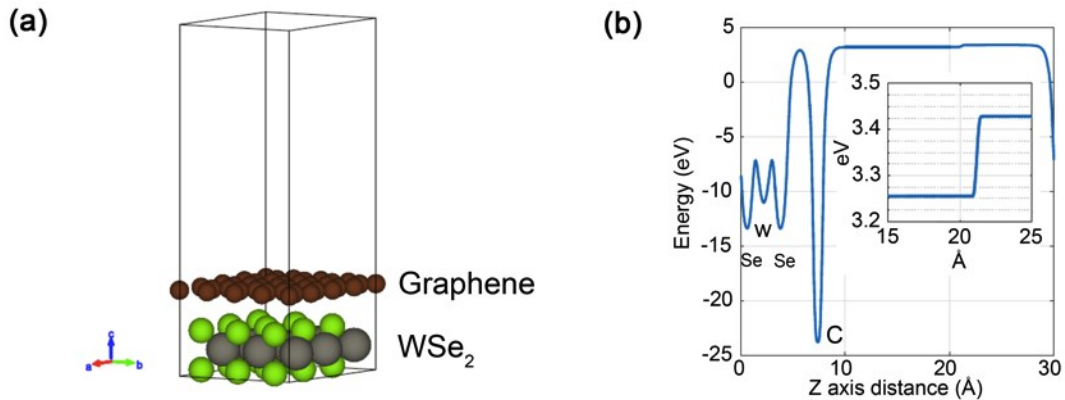
**Supplementary Table 2.** Computed dependence of electron affinity plus bandgap of WSe<sub>2</sub> ( $X_{WSe_2} + E_g$ ), unintentional doping of WSe<sub>2</sub> ( $N_A$ ), carrier density of WSe<sub>2</sub> after charge transfer between WSe<sub>2</sub> and EG<sub>PH</sub> ( $N_{C,WSe_2-EG_{PH}}$ ), and carrier density of WSe<sub>2</sub> after charge transfer between WSe<sub>2</sub> and EG<sub>FH</sub> ( $N_{C,WSe_2-EG_{FH}}$ ) on electron affinities of EG<sub>PH</sub> ( $X_{EG_{PH}}$ ) and EG<sub>FH</sub> ( $X_{EG_{FH}}$ ), respectively. An error range of  $\pm 0.1$ eV for the input parameters is considered.



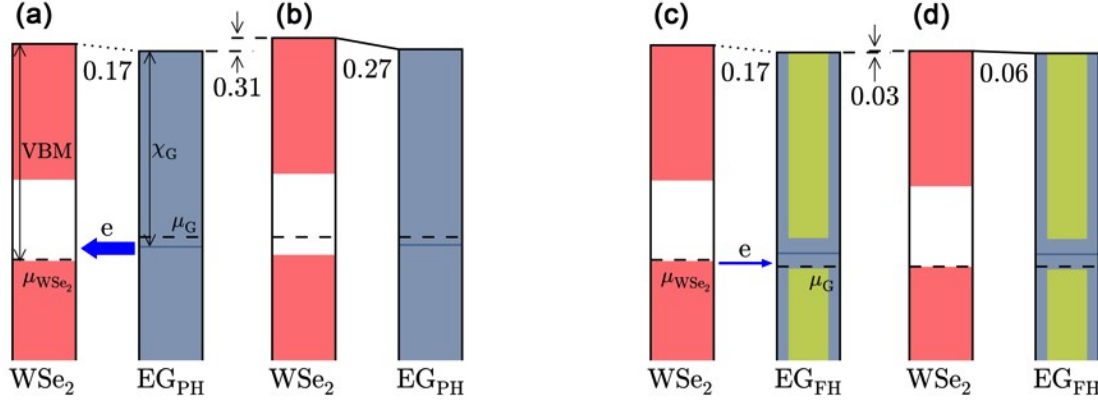
**Supplementary Figure 1.** The G peak positions from the same as-grown graphene and the graphene samples from the 800 °C and 930 °C  $\text{WSe}_2$  growth that provide the information of the 2D peaks in the Figure 2 c and 2d.



**Supplementary Figure 2.** (a) and (b) are linear plots of the  $I$ - $V$  curves from graphene and  $\text{WSe}_2$ -graphene samples, respectively, presented in the Figure 4a. (c) A comparison of  $I$ - $V$  curves measured on multiple 1L  $\text{WSe}_2$  domains grown on  $\text{EG}_{\text{PH}}$  and  $\text{EG}_{\text{FH}}$  shows a clear reduction of turn-on voltage for the  $\text{WSe}_2\text{-EG}_{\text{FH}}$  case.



**Supplementary Figure 3.** (a) Plane averaged local electric potential energy of electrons along the stacking direction. (b) After dipole correction, a difference on vacuum energy above both sides of 0.17 eV is observed (zoomed inset).



**Supplementary Figure 4.** Band alignment of WSe<sub>2</sub> and EG<sub>PH</sub> (a) before charge transfer (including computed intrinsic dipole 0.17 eV), and (b) after charge transfer. Band alignment of WSe<sub>2</sub> and EG<sub>FH</sub> (c) before charge transfer (including the intrinsic dipole), and (d) after charge transfer. Monolayer and bilayer graphene models are employed for EG<sub>PH</sub> and EG<sub>FH</sub> respectively, based on LEEM observations. Green shades in (c) and (d) represent conduction/valence subbands of bilayer graphene. The numerical values show various vacuum level differences, in units of eV.

### Computational methods for the intrinsic dipoles between WSe<sub>2</sub> and graphene

The density functional theory (DFT) calculation are performed by Vienna ab-initio simulation package (VASP)<sup>2</sup> with the projector-augmented wave (PAW) method.<sup>3</sup> The local density approximation (LDA)<sup>4</sup> is used to describe the exchange-correlation functional with the partial core correction included. Spin polarization and spin-orbit coupling are applied. The stable phase of the monolayer WSe<sub>2</sub> is trigonal prism structure.<sup>5</sup> The optimized planar lattice constant of WSe<sub>2</sub> is 3.25 Å, and the optimized planar lattice constant for monolayer graphene is 2.45 Å. In order to fit the lattice constant, a super cell with 3×3 WSe<sub>2</sub> unit cells and 4×4 graphene unit cell is used, and a compressive strain of 0.4 % is applied to graphene, as the electronic behaviors of TMD are very much susceptible to lattice strain. The super cell is shown in Figure 2a. The wave functions are expanded in plane waves with a kinetic energy cutoff of 500 eV, and the convergence criteria for the electronic relaxation is 10<sup>-5</sup> eV. Integration over the Brillouin zone is performed with a gamma-centered 6×6×1 Monkhorst-Pack k-point mesh for ionic and electronic optimization. A vacuum region of about 15 Å normal to the surface is added to minimize the interaction between adjacent slabs (Figure S3a). Dipole correction on the stacking direction is used in systems to reveal the dipole within the two layers caused by the Fermi-level alignment. The local density approximation (LDA) is found to be suitable for studying the metal-TMD contact.<sup>6</sup> The generalized gradient approximation (GGA)<sup>7</sup> with the DFT-D2 method for van der Waals (vdW) corrections<sup>8</sup> is also used to cross-check the structural accuracy. We find that GGA results with vdW corrections are in overall agreement with LDA results. Both the LDA method and the GGA+vdW method result in a similar

structure with a distance of  $\sim 3.5$  Å between graphene and TMD, indicating a secondary bond interaction. The energy difference between the vacuum regions on the both sides of the contact system is the dipole induced by the contact. The vacuum energy level above WSe<sub>2</sub> is 0.17 eV higher than that above graphene, indicating a dipole from graphene towards the WSe<sub>2</sub> (Figure S3b).

### Computation of WSe<sub>2</sub> doping density and charge densities, and dependence on parameters

For the computation of charge transfer and band alignment, we take the doping densities of EG<sub>PH</sub> and EG<sub>FH</sub> from our experimental values, as discussed in the main text. Parameters in the computation are the electron affinities for monolayer and bilayer graphene, with nominal values of 4.57 eV and 4.71 eV, respectively, as known from prior experiments.<sup>9</sup> We take the sum of the electron affinity plus band gap of the WSe<sub>2</sub>,  $X_{\text{WSe}_2} + E_g$ , to be an unknown in the computation, since a value for this sum is not accurately known from prior work (only the sum is considered here since the electron occupation in the conduction band of the WSe<sub>2</sub> is negligible). A second unknown is the unintentional doping density of WSe<sub>2</sub>. Then, using the two measured work function differences for WSe<sub>2</sub> on both EG<sub>PH</sub> and EG<sub>FH</sub> compared to the bare EG<sub>PH</sub> and EG<sub>FH</sub>, we can determine values for the two unknown parameters. The carrier densities for the WSe<sub>2</sub> on both EG<sub>PH</sub> and EG<sub>FH</sub> after charge transfer are then a byproduct of the computation. Table S2 shows dependence of these quantities on the input parameter values. In all cases, the carrier densities of WSe<sub>2</sub> in WSe<sub>2</sub>-EG<sub>PH</sub> are very much greater than those of WSe<sub>2</sub> in WSe<sub>2</sub>-EG<sub>FH</sub>, consistent with the observed differences in the CAFM I-V results.

We note that the doping density values in Table S2 are all the same, reflecting a tight constraint on this value. This constraint arises from charge transfer between the WSe<sub>2</sub> and the EG<sub>PH</sub>. As pictured in Figure S4a and 4b, since the Fermi energies of the EG<sub>PH</sub> and WSe<sub>2</sub> are relatively far apart prior to charge transfer, and hence the Fermi energy of the WSe<sub>2</sub> ends up well within its band gap after the transfer, then the p-type doping density in the WSe<sub>2</sub> is directly determined by the doping density of the EG together with the difference between the electron affinity of the EG<sub>PH</sub> and the  $X_{\text{WSe}_2} + E_g$  value of the WSe<sub>2</sub>. The resulting carrier densities for the WSe<sub>2</sub> on EG<sub>PH</sub> are negligible, again since the resulting WSe<sub>2</sub> Fermi energy is well within the gap. On the other hand, for the WSe<sub>2</sub> on EG<sub>FH</sub>, their Fermi energies are relatively close prior to charge transfer, as pictured in Figure S4c and 4d. The resulting Fermi energy for the WSe<sub>2</sub> on EG<sub>FH</sub> ends up near or within the valence band even after the charge transfer, with concomitant large carrier density, and the value of the WSe<sub>2</sub> doping density is not so tightly constrained in this part of the problem.

We have also considered the effect on the computed carrier densities of variation in the  $EG_{\text{PH}}$  and  $EG_{\text{FH}}$  doping density values, as well as variation of the measured work functions differences within their experimental error ranges. Doping densities of  $(4 \pm 1) \times 10^{12} \text{ cm}^{-2}$  for  $EG_{\text{PH}}$  and  $(1.5 \pm 0.2) \times 10^{13} \text{ cm}^{-2}$  for  $EG_{\text{FH}}$  are typical measured in our samples. Considering the variations of these doping densities, the carrier density of  $\text{WSe}_2$  on  $EG_{\text{FH}}$  after charge transfer is computed to range from  $2.5 - 3.0 \times 10^{12} \text{ cm}^{-2}$  while the carrier density of  $\text{WSe}_2$  on  $EG_{\text{PH}}$  after transfer is always less than  $10^7 \text{ cm}^{-2}$ , i.e. its Fermi is well within the bandgap. For the measured error ranges ( $\pm 0.03 \text{ eV}$ ) on the work function differences, performing computations at the bounds of these values produces carrier densities in the  $\text{WSe}_2$  on  $EG_{\text{FH}}$  compared to  $\text{WSe}_2$  on  $EG_{\text{PH}}$  that continue to differ by more than a factor of  $10^4$ , for all cases.

#### Reference:

- 1 Y.-C. Lin, R. K. Ghosh, R. Addou, N. Lu, S. M. Eichfeld, H. Zhu, M.-Y. Li, X. Peng, M. J. Kim, L.-J. Li, R. M. Wallace, S. Datta and J. A. Robinson, *Nat. Commun.*, 2015, **6**, 7311.
- 2 G. Kresse and J. Furthmüller, *Phys. Rev. B*, 1996, **54**, 11169–11186.
- 3 G. Kresse and D. Joubert, *Phys. Rev. B*, 1999, **59**, 1758–1775.
- 4 D. M. Ceperley and B. J. Alder, *Phys. Rev. Lett.*, 1980, **45**, 566–569.
- 5 C. Gong, H. Zhang, W. Wang, L. Colombo, R. M. Wallace and K. Cho, *Appl. Phys. Lett.*, 2013, **103**, 053513.
- 6 C. Gong, L. Colombo, R. M. Wallace and K. Cho, *Nano Lett.*, 2014, **14**, 1714–20.
- 7 J. P. Perdew, K. Burke and M. Ernzerhof, *Phys. Rev. Lett.*, 1997, **78**, 1396–1396.
- 8 G. Makov and M. Payne, *Phys. Rev. B*, 1995, **51**, 4014–4022.
- 9 Y.-J. Yu, Y. Zhao, S. Ryu, L. E. Brus, K. S. Kim and P. Kim, *Nano Lett.*, 2009, **9**, 3430–3434.